*Polymer Science, Ser. A, Vol. 44, No. 6, 2002, pp. 581–592. Translated from Vysokomolekulyarnye Soedineniya, Ser. A, Vol. 44, No. 6, 2002, pp. 946–959.*




# Poly(methyl methacrylate) and Poly(butyl methacrylate) Swelling in Supercritical Carbon Dioxide and the Formation of a Porous Structure[1]

**M. O. Gallyamov*[2], R. A. Vinokur**, L. N. Nikitin**, E. E. Said-Galiyev**, A. R. Khokhlov**, and K. Schaumburg*****

** Faculty of Physics, Moscow State University, Leninskie gory, Moscow, 119899 Russia*

*** Nesmeyanov Institute of Organoelement Compounds, Russian Academy of Sciences, ul. Vavilova 28, Moscow, 119991 Russia*

**** Center for Interdisciplinary Studies of Molecular Interactions, Department of Chemistry, University of Copenhagen, Universitetsparken 5, DK-2100, Copenhagen, Denmark*

Received July 4, 2001;
Revised Manuscript Received October 11, 2001

**Abstract**—The swelling of poly(methyl methacrylate) and poly(butyl methacrylate) bulk samples in supercritical carbon dioxide was studied in situ. It was shown that the optical technique used to monitor the sorption process in the supercritical fluid allowed the diffusion coefficients of carbon dioxide molecules in the samples to be determined both by analyzing the movement of optical boundaries and from volume swelling kinetics. The diffusion coefficients in poly(methyl methacrylate) and poly(butyl methacrylate) were assumed to be concentration-dependent, and the models proposed were found to explain the formation of optical boundaries that had been detected experimentally in these samples. The experimental data were fitted to the results of computer simulation of the sorption process. Pore formation in the samples upon desorption of carbon dioxide in different exposure and decompression modes was visualized using optical (in situ) and atomic-force (ex situ) microscopy. The plasticizing effect of $CO_2$ on the pore formation process is discussed.

## INTRODUCTION

The behavior of various classes of polymers in supercritical fluids, especially in supercritical carbon dioxide, has become a subject of considerable interest in recent years [1, 2]. This increased attention is due to the fact that supercritical $CO_2$ is a solvent or plasticizer for a variety of polymers, having such advantages over conventional solvents (plasticizers) as low cost, environmental friendliness, incombustibility, and ease of removal from a polymer after completion of a process.

On the other hand, the interest concerning this fluid is due to the possibility of altering the morphological and functional properties of polymers by holding them in supercritical $CO_2$ and the ability of the latter to extract low-molecular-mass compounds including water, residual solvents, and monomers from a polymer [3]. In addition, the possibility of forming a porous structure in polymers by varying the pressure and temperature of supercritical $CO_2$ upon exposure and decompression seems quite promising as it can be used to manufacture porous adsorbent, filter, membrane, etc. materials.

However, successful implementation of such technologies in practice requires detailed study both of swelling mechanisms and pore formation upon sorption and desorption of supercritical fluid $CO_2$.

The swelling of poly(dimethylsiloxane)s in the plastic state in supercritical $CO_2$ was studied by Royer *et al.* [4]. The equilibrium swelling degrees and diffusion coefficients were determined by monitoring the dynamics of displacement of the physical boundary of a swelling polymer placed in a test tube. Von Schnitzler and Eggers [5] analyzed the mass and volume swelling kinetics in supercritical $CO_2$ for PET samples in the form of extended cylinders, determined the equilibrium diffusion coefficients, and measured sorption isotherms.

In this work, we studied the swelling of parallelepiped-shaped poly(methyl methacrylate) (PMMA) and poly(butyl methacrylate) (PBMA) samples in supercritical $CO_2$ and analyzed the kinetics of both an increase in volume and movement of optical boundaries formed in the samples during the sorption of $CO_2$.

[1] This work was supported by the Russian Foundation for Basic Research, project no. 01-03-32766a.
[2] E-mail: glm@spm.phys.msu.su

## EXPERIMENTAL

Experiments in supercritical $CO_2$ ($p_{cr}$ = 7.38 MPa, $T_{cr}$ = 31.1°C, $\rho_{cr}$ = 470 kg/m$^3$) were made in a special unit designed for the purpose on the basis of one described earlier [6, 7]. To create pressure in the range 9–15 MPa, a syringe pressure generator (working volume 150 ml) was used. Carbon dioxide was supplied to a reaction cell through a set of valves. The pressure generator and cell were equipped with mechanical pressure gauges to monitor the pressure and to control the gas inflow–outflow system.

The task of in situ studying processes in supercritical $CO_2$ demanded the development of a special high-pressure cell. It represented a container ~10 cm$^3$ in volume made of stainless steel. The wall thickness selected was several times as high as that predicted to withstand a pressure of 15 MPa, thus allowing heaters, capillary inlet tubes, and a temperature probe to be accommodated in the cell case. The adaptive proportional–integral–differential temperature control had an accuracy of better than ±0.2°C. The experiments were carried out at $T$ = 38–65°C. An electronic pressure transducer allowed pressure in the chamber to be measured with an accuracy of 0.1 MPa.

Indium-sealed, 10-mm thick quarts optical windows were used to make an optical channel in the high-pressure chamber. The swelling of samples and the motion of an optical boundary was observed through them with an optical microscope equipped with a Logitech QuickCam Pro digital video camera. Information was recorded as a raster image (640 × 480 points) onto a computer hard disk in prescribed time intervals (from 10 to 60 s). A two-color superbright light-emitting diode was used as a light source.

The unit was operated by a personal computer (Pentium III) equipped with a DT-322 (Data Translation Inc., USA) data acquisition board. Special software was developed to perform real-time experiments.

Experiments on the sorption of $CO_2$ were performed as follows. A polymer sample as a parallelepiped with an edge length of 1–5 mm was mounted in the cell, the cell was sealed, and temperature was elevated to a prescribed value. Then, by increasing the syringe pressure, supercritical $CO_2$ was allowed into the cell and the sample was viewed with a video camera through the cell optical channel. This experimental scheme made it possible to study the kinetics of changes in linear dimensions of polymer samples in the supercritical fluid, to monitor the propagation of optical boundaries, and to observe pore formation upon decompression.

Changes in the surface morphology of samples after their exposure to the supercritical fluid were examined by atomic-force microscopy (AFM). AFM experiments were performed in air with a Nanoscope-IIIa (Digital Instruments, USA) scanning probe microscope in the contact mode at a constant probing force (a few nanonewtons). Commercial Nanoprobe cantilevers (spring constant 0.32 N/m) with silicon nitride tips were used. The probe microscope was equipped with a D-scanner (dynamic range $15 \times 15 \times 4$ μm$^3$) calibrated with a calibration grid made available from the manufacturer. AFM images were recorded with a horizontal-scan frequency of 5–15 Hz at an information density of 512 × 512 points. No pretreatment of sample surfaces prior to AFM studies was made. AFM images and computer-simulated images were plotted with the use of the Femtoscann Online v. 1.2 image processing program (the Advanced Technology Center, Russia) [8].

The polymeric materials used had the following characteristics. PBMA: $M_w$ = 2236000, $M_n$ = 861400, $M_w/M_n$ = 2.6 (as determined with GPC), $\rho$ = 1070 kg/m$^3$, $T_g$ = 27°C; PMMA: $M_w$ = 4098000, $M_n$ = 2530400, $M_w/M_n$ = 1.6 (GPC), $\rho$ = 1170 kg/m$^3$, $T_g$ = 114°C.

Carbon dioxide of high purity grade (>99.997%, GOST (State Standard) 8050-85, $O_2$ 0.0002%, $H_2O$ 0.001%) was used without further purification.

## RESULTS AND DISCUSSION

PBMA and PMMA samples were selected for studying swelling under supercritical conditions for the reason that they are capable of sorbing $CO_2$ in an amount of up to tens of weight per cent; indeed, it has been shown [9–11] that the equilibrium degree of swelling of PMMA in supercritical $CO_2$ can be as high as 20 wt % and greater and PBMA swelling is even more effective according to our observations.

### *Formation and Movement of Optical Boundaries in Samples*

The procedure for determining diffusion coefficients by analyzing the kinetics of motion of the optical boundary formed under certain conditions in an optically transparent sample subjected to swelling or dissolution is widely used in the practice of diffusion studies on polymers [12, 13]. We first applied this approach to analyze sorption under supercritical fluid conditions.

Figure 1 shows the photographs of the steps of $CO_2$ sorption by the polymers as taken with an optical microscope. It is seen that a distinct optical boundary (dark, relatively narrow band) is formed in the PMMA sample (Fig. 1A), which moves (as $CO_2$ is sorbed) from the surface to the center of the sample. The sample regions on both sides of the boundary are substantially lighter as compared to the boundary. In this case, the motion of the optical boundary can be monitored up to its contraction to a point in the center.

The picture observed for PBMA (Fig. 1B) is somewhat different. Formed here are darkened areas characterized by a sharp boundary that also moves (as sorption advances) to the sample center (reaching the central region of the sample, the boundary becomes hardly

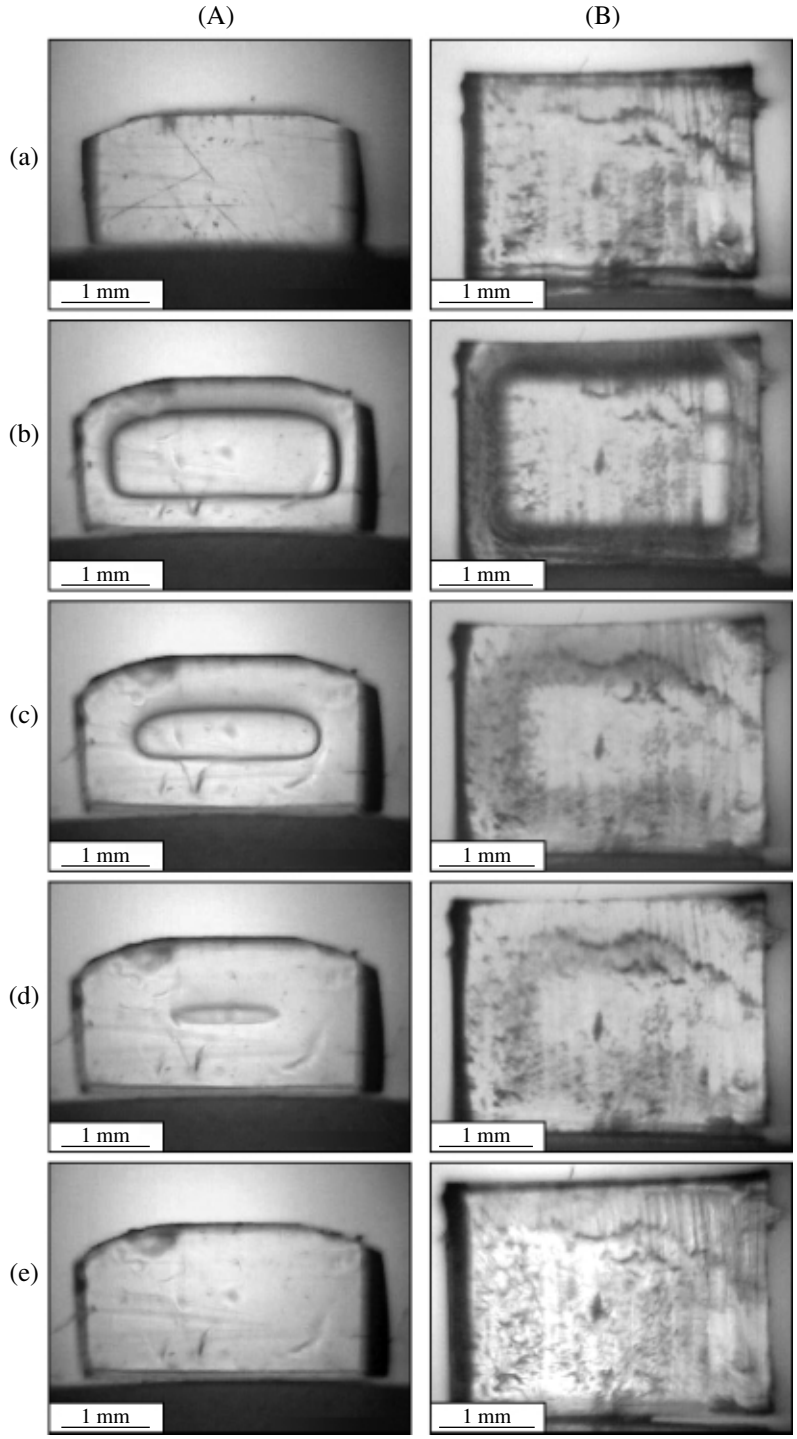


**Fig. 1.** Steps of $CO_2$ sorption by (A) PMMA and (B) PBMA samples during exposure under supercritical conditions at a temperature of 38°C and a pressure of 12.5 MPa. Exposure time of (A): (a) 0, (b) 20, (c) 40, (d) 60, and (e) 80 min and (B): (a) 0, (b) 2, (c) 4, (d) 6, and (e) 8 min.

distinguishable). The entire region between the optical and physical boundaries of the sample appears to be substantially darker than the central region. This effect is especially pronounced in the initial sorption step; further, the darkened areas gradually become lighter.

Typical results obtained by treating the rate of motion of optical boundaries in PMMA and PBMA samples are presented in Fig. 2a. To measure the distance traveled by a boundary, the sample center was taken as a reference point. It is seen that the square dis-

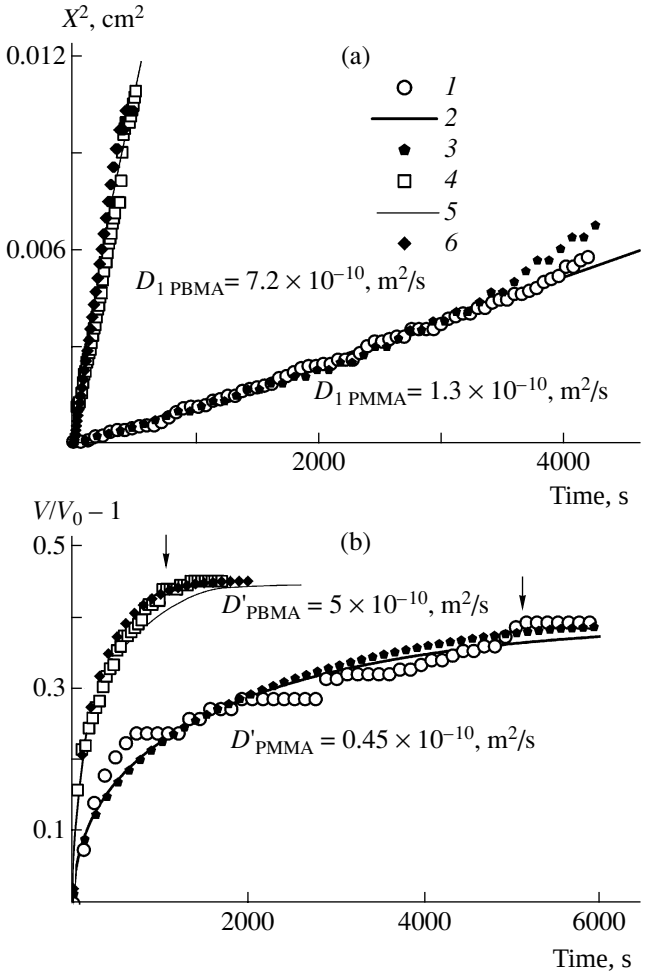


**Fig. 2.** Typical results obtained for propagation of optical boundaries in (*1–3*) PMMA and (*4–6*) PBMA samples and for their swelling upon exposure to supercritical $CO_2$ (temperature 38°C, pressure 9 MPa): (*1*, *4*) experimental data; (*2*, *5*) theoretical approximations of the experimental data according to Eqs. (2) and (10), respectively; (*3*, *6*) computer simulation data (corresponding to the $D'$ values calculated with Eq. (10)) for PMMA ($c_x/c_0$ = 0.7, $D_1/D_2$ = 20) and for PBMA ($D_1/D_2$ = 7.5) models. (a) Time dependence for the squared distance $X^2$ traveled by optical boundaries; (b) time dependence for the relative increment in sample volume ($V_0$ is the sample volume before swelling).

tance covered as a function of time is approximated with good accuracy by a straight line for both polymers.

It is known that, if the diffusion coefficient is invariable, the initial concentration distribution in a sample smooths with time: the characteristic sizes of regions with significant changes in concentration and concentration gradient increase. In the case of sorption, the distribution of concentration gradient is described by Gaussian curves with a maximum at the physical boundary of the sample and the width increasing proportionally to $t^{1/2}$. If the refractive index depends on the sorbate concentration, it is possible that darkened areas with a sharp transition region (optical boundary) will be formed in a sorbing sample, but the width of the transition region increases with time proportionally to $t^{1/2}$ and the optical boundary smears.

Since sharp, moving optical boundaries without diffusional smearing are observed in the samples (Fig. 1), the mechanism of their formation should be interpreted in terms of the assumption of a pronounced concentration dependence of the $CO_2$ diffusion coefficient in PMMA and PBMA.

### *Formation of the Optical Boundary in PMMA Samples*

**The Stefan problem.** We propose the following model to explain the formation of the optical boundary in the case of PMMA.

Since the experiments were made at a temperature below the $T_g$ of PMMA, the sample placed in supercritical $CO_2$ initially occurred in the glassy state. Further, with the progress of $CO_2$ sorption, the polymer must undergo a transition to the rubbery state according to the published data [14, 15]. It may be assumed that the transition took place in each region of the sample upon exceeding the local concentration of $CO_2$ sorbed over a certain limiting value $c_x$. Let us also assume that the diffusion coefficients of $CO_2$ in the rubbery polymer, $D_1$, and in the glassy polymer, $D_2$, are different, being $D_1 > D_2$ (in the simplest case, it may be assumed that $D_1$ and $D_2$ do not depend on concentration). Thus, the simplest pattern of diffusivity in PMMA is as follows:

$$D(c) = \begin{cases} D_1 = \text{const} & \text{at} \quad c > c_x \\ D_2 = \text{const} & \text{at} \quad c < c_x \end{cases} \qquad D_1 > D_2. \quad (1)$$

Then, the analysis reduces to the well-known Stefan problem [16, 17], whose solution (the Neumann solution for a semi-infinite medium) predicts a linear relation between the squared displacement of the front of constant concentration $c_x$ and time

$$X^2 = \alpha D_1 t. \quad (2)$$

The dimensionless proportionality factor $\alpha$ in this case is a root of the equation

$$\frac{\frac{c_x}{c_0} - 1}{\operatorname{erf}\left(\frac{\sqrt{\alpha}}{2}\right)} e^{\frac{-\alpha}{4}} + \frac{\frac{c_x}{c_0}}{\sqrt{\frac{D_1}{D_2}}\left(1 - \operatorname{erf}\left(\frac{\sqrt{\alpha}}{2}\frac{D_1}{D_2}\right)\right)} e^{\frac{-\alpha}{4}\frac{D_1}{D_2}} = 0, \quad (3)$$

where erf($x$) is the error function and $c_0$ is the $CO_2$ concentration at the physical boundary of a polymer.

Thus, the α value is uniquely determined by two ratios $D_1/D_2$ and $c_x/c_0$.

The region of the propagating front of constant concentration $c_x$ is characterized by a finite jump in the concentration gradient, whose value is defined by the relationship

$$D_1\frac{dc_1}{dx} = D_2\frac{dc_2}{dx}, \quad (4)$$

where $c_2$ and $c_1$ are the concentrations ahead of and behind the front, respectively. From Eq. (4), it is seen that the concentration gradient in the region immediately before the front is significant when $D_1$ and $D_2$ considerably differ. If the refractive index is concentration-dependent, this leads to the formation of an optical boundary in this region [12, 13]. Indeed, the deviation of a light beam propagating in an optically nonuniform system over a small distance *dz* is defined by [18]

$$d\alpha = \frac{|\nabla_\perp n|}{n}dz, \quad (5)$$

where $\nabla_\perp n$ is the projection of the refraction index gradient onto the direction of the principal normal to the beam trajectory. Beams passing near and parallel to the front of constant concentration $c_x$ will substantially deviate, producing a darkened area on the sample image. Such darkened areas will be localized only in a rather narrow region immediately before the front, where the corresponding component of concentration gradient has a significant value according to Eq. (4). Then, the forming optical boundary will appear as a relatively narrow dark band, as we find in PMMA samples (Fig. 1A). Therefore, we assume that Eq. (1) is a good approximation for the actual concentration dependence of the diffusion coefficient in PMMA. The movement of an optical boundary will be determined by the propagation of the front of constant concentration $c_x$ and, for this reason, must obey relationship (2), which is indeed observed in the experiment (Fig. 2a).

The analysis of the kinematics of the optical boundary allows the diffusion coefficient $D_1$ to be determined provided that the value of α in relationship (2) is known. In order to determine this parameter from Eq. (3), it is necessary to know the ratios $c_x/c$ and $D_1/D_2$. Their determination required computational simulation to be performed for fitting to the experimental results.

**Computer simulation.** The computational modeling of the process was based on the following premises.

(1) The diffusion equation was approximated by a finite-difference scheme [19] of the first order in time (the derivative only with respect to one spatial coordinate is written in an explicit form)

$$c_{ijk}^{t+1} = c_{ijk}^{t} + M\left(\frac{D(c_{i+1jk}^{t}) + D(c_{ijk}^{t})}{2}(c_{i+1jk}^{t} - c_{ijk}^{t}) - \frac{D(c_{ijk}^{t}) + D(c_{i-1jk}^{t})}{2}(c_{ijk}^{t} - c_{i-1jk}^{t})\right) + \ldots, \quad (6)$$

where *c* is the normalized concentration in grid points and *D* is the concentration-dependent diffusion coefficient. The parameter *M* of the scheme was selected on the basis of the stability condition $MD \le 1/6$. The subscripts *ijk* and *t* denote grid points and time, respectively. At the initial point of time, $c_{ijk} = 0$ in all grid points, and $c_{ijk} = 1$ at any time in the boundary points.

(2) The concentration dependence of *D* was described in accordance with the model proposed for PMMA (Eq. (1)) and PBMA.

(3) The concentration dependence of the refractive index in (Eq. (5) was determined using the Lorentz–Lorenz equation [18]

$$\frac{n^2 - 1}{n^2 + 1} = \frac{4}{3}\pi\sum_i N_i\alpha_{el}^i \quad (7)$$

by successively writing it for pure components and their mixture. Here, $N_i$ is the number of particles in unit volume and $\alpha_{el}^i$ is the electronic polarizability of a particle of the *i*th type. The set of equations taking into account the equilibrium degree of swelling of samples in supercritical $CO_2$ allows the refractive index of the mixture to be expressed in an explicit form through the normalized local concentration of the sorbate (Eq. (6)), as well a through the refractive indexes of a polymer ($n = 1.49$ [20] was used for both PMMA and PBMA) and supercritical $CO_2$ (the value of $n = 1.11$ at $p = 9$ MPA and $T = 42°C$ [21] was used).

(4) The darkening intensity was assumed to be proportional to the total deviation of a ray propagating in a plane-parallel beam along one of the sample axes and was calculated by numerical integration of Eq. (5).

The numerical experiment resulted in images of optical boundaries forming and propagating in the samples modeled (Fig. 3); time dependence for the distance covered by an optical boundary (Fig. 2a) and calculated (by numerical integration of concentration over sample volume) time dependence of the sorbate mass (Fig. 2b).

**Determination of the diffusion coefficient from kinetics data on the movement of an optical boundary.** The ratios $c_x/c_0$ and $D_1/D_2$ required for calculating the diffusion coefficient $D_1$ according to Eqs. (2) and (3) were found by the iteration procedure.

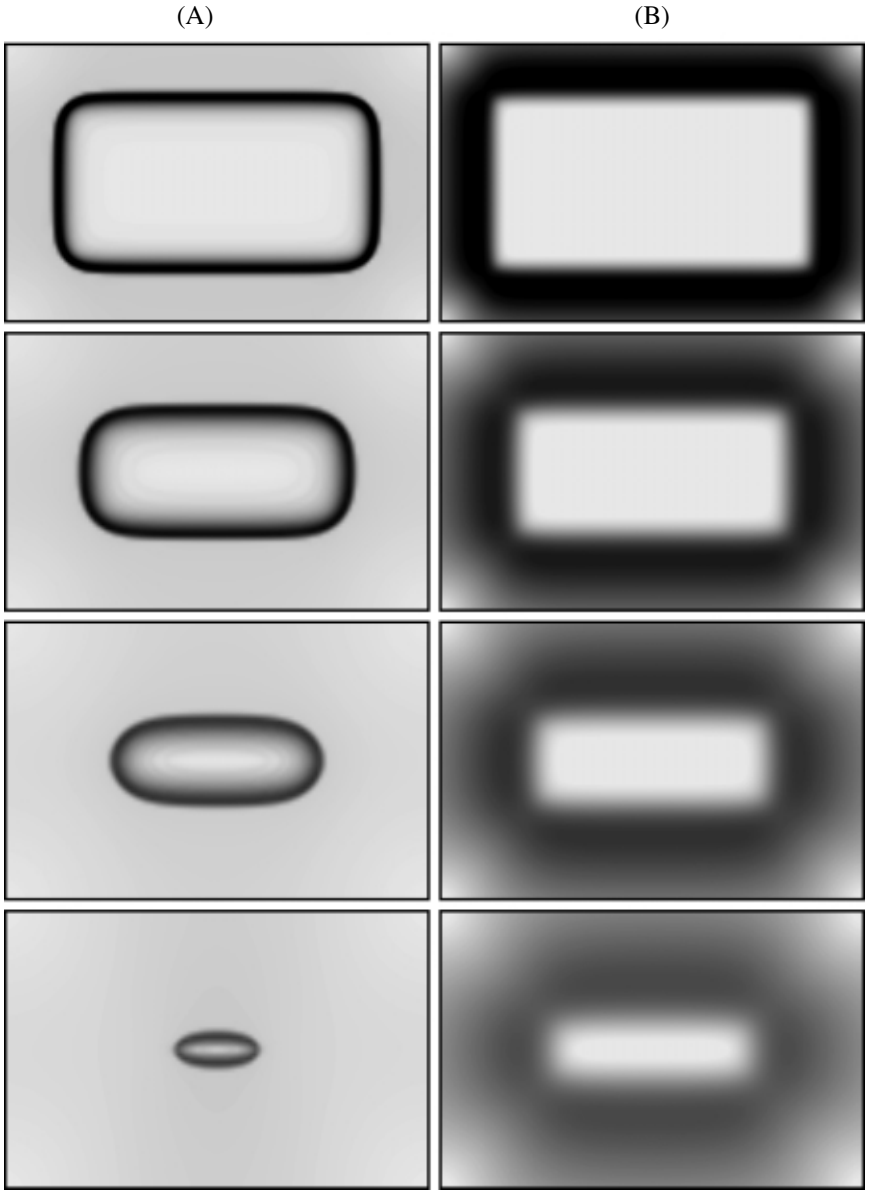


**Fig. 3.** Results of computer simulation of the processes of formation and propagation of optical boundaries in polymer samples for (A) the PMMA model (Eq. (1)) at $c_x/c_0 = 0.7$ and $D_1/D_2 = 20$ and (B) the PBMA model (Eq. (9)) at $D_1/D_2 = 7.5$. The images for each set were calculated in equal time intervals.

For preliminary estimation of $c_x/c_0$, the following approach was used. Since the process of propagation of optical boundaries in PMMA can be followed up to the moment of their merging in the sample center and disappearance, it is experimentally feasible to measure the propagation time $t$. At the moment when the optical boundaries merge, the concentration in the center of the sample is equal to $c_x$. On the other hand, as known from the diffusion theory, the sorption behavior of a rectangular-shaped sample with linear dimensions of $l_x \times l_y \times l_z$ placed in a medium with a certain sorbate concentration is described by a solution to the diffusion equation with zero initial and constant boundary conditions, the following relationship holding for sorbate concentration in the center of the parallelepiped [16, 17]:

$$\frac{c_x}{c_0} = 1 - \frac{64}{\pi^3}\sum_{i=0}^{\infty}\frac{(-1)^i}{2i+1}\exp\left(\frac{-(2i+1)^2\pi^2 D't}{l_x^2}\right) \times \sum_{j=0}^{\infty}\frac{(-1)^j}{2j+1}\exp\left(\frac{-(2j+1)^2\pi^2 D't}{l_y^2}\right) \times \sum_{k=0}^{\infty}\frac{(-1)^k}{2k+1}\exp\left(\frac{-(2k+1)^2\pi^2 D't}{l_z^2}\right). \quad (8)$$

Measuring the front propagation time $t$ (typical values are 1–1.5 h) for the known linear dimensions of samples ($\sim 2 \times 2 \times 4$ mm$^3$) and using the values of the apparent diffusion coefficient $D'$ estimated by the volume swelling technique ($\simeq 0.7 \times 10^{-10}$ m$^2$/s, see below), we found that the typical values of the sought quantity $c_x/c_0$ lie in the range 0.7–0.9 according to Eq. (8). Note that Eq.(8) is valid in the approximation of a constant diffusion coefficient; therefore, the value of $c_x/c_0 = 0.8$ was used only as a preliminary estimate that needs to be further refined.

Control criteria in the iterative determination of $c_x/c_0$ and $D_1/D_2$ were the results of fitting, first, the calculated degree of swelling of a sample at the front merging time $t$ to the one measured experimentally and, second, the shape of the optical boundary on the experimental images to that obtained by computer simulation.

The first control criterion is due to the fact that at the moment of front merging (when the sorbate concentration in the sample center is equal to $c_x$), the degree of swelling of the sample is determined by the parameters sought and the ratios between linear dimensions of the sample. Experimentally, it was found that on average (with reference to the scatter due to the difference in the ratio of linear dimensions of the samples examined) this moment corresponds to attaining 90–98% of the equilibrium degree of swelling.

The second control criterion is due to the fact that, according to Eq. (4), the shape of the simulated optical boundary is determined by $D_1/D_2$ and $c_x$. The iterative procedure allowed a refined estimate to obtained: $c_x/c_0 \simeq 0.7$, $D_1/D_2 > 10$. At these values, the error of determination of $\alpha$ using Eq. (3) is primarily due to the error of $c_x/c_0$ owing to a higher sensitivity of $\alpha$ to variation in this parameter; for example, as $c_x/c_0$ increases within 0.6–0.8 at a fixed value of $D_1/D_2 = 20$, the factor $\alpha$ decreases from 1.0 to 0.4 and as $D_1/D_2$ increases from 10 to 100 at fixed $c_x/c_0 = 0.7$, $\alpha$ increases from 0.63 to 0.74 (when $D_1/D_2$ is further increased, $\alpha$ tends to the limiting value of 0.75).

Thus, under the conditions $c_x/c_0 \simeq 0.7$ and $D_1/D_2 > 10$ found, the law of motion of the $c_x$ front (optical boundary) (Eq. (2)) is determined by the value of $D_1$ and is almost independent of $D_2$ (since $\alpha$ slightly changes upon variation in $D_1/D_2$). At $c_x/c_0 = 0.7$ and $D_1/D_2 = 20$, the value of $\alpha$ will be 0.7; it is this value that we will use to determine the coefficient $D_1$ from experimental data (according to Eq. (2)). Since the procedure does not allow $D_1/D_2$ to be estimated with appropriate accuracy, the coefficient $D_2$ was not calculated and will not be further discussed.

The images of optical boundaries obtained by computer simulation for PMMA are shown in Fig. 3A. It is seen that there is qualitative agreement with the experimental results (cf. the images in Fig. 1A). Figure 2a depicts the numerically modeled time dependence for the coordinate of the front of $c_x$. It is seen that it approximates well the experimental data and follows law (2) up to the moment of front contraction at the sample center.

### *Formation of an Optical Boundary in PBMA Samples*

Since PBMA samples initially occurred in the rubbery state (at temperatures above $T_g$) in the experiments, the sorption process has a somewhat different character as compared to PMMA.

As has already been noted, the fact of experimental observation of propagating optical boundaries leads to the assumption that the diffusion coefficient depends on concentration, $D = D(c)$. The shape of the optical boundary and fitting to the computational simulation results suggest that the diffusion coefficient in PBMA increases gradually (not in a jumpy manner as in PMMA) as $CO_2$ is sorbed. Owing to the complexity of the use of analytic procedures in solving the diffusion problem, we attempted computational simulation for fitting to experimental data in this case as well.

**Computer simulation.** Modeling was based on the same premises as in the case of diffusion in PMMA, except for the assumption on the character of concentration dependence for the diffusion coefficient.

As the simplest model of the function $D(c)$ for PBMA, we selected linear growth with increasing sorbate concentration:

$$D(c) = D_2 + (D_1 - D_2)c, \quad D_1 > D_2, \qquad (9)$$

where $c$ is the sorbate concentration normalized to the equilibrium value. Qualitative agreement between simulation results and the experimental data was achieved by varying $D_1/D_2$. Such an analysis allowed the suggestion to be made that the $D_1/D_2$ ratio for PBMA lies in the range 5–10. Under these conditions, the images obtained by computational simulation have darkened areas with a relatively sharp boundary (Fig. 3B) which qualitatively resemble those observed experimentally (Fig. 1B). Numerical analysis shows that the boundary distribution law in this case (as a reference, we took the point at which the intensity of darkening is half its maximum value, as in the real experiment) also has the form defined by Eq. (2) (Fig. 2a). The sorbate concentration in the boundary localization region turned out to be 2–4% of the equilibrium value. The factor $\alpha \simeq 3$ (at $D_1/D_2 \simeq 7$ or greater) was determined; it was this value that we used to calculate the coefficient $D_1$ in PBMA from the experimental data using Eq. (2).

### *Analysis of Volume Swelling Kinetics*

The values obtained for $D_1$ were compared with the results of the analysis of the volume swelling kinetics. From Fig. 1, it is seen that the linear dimensions of samples increase during their exposure to supercritical $CO_2$. Our scheme used to monitor the swelling of a

**Table 1.** Equilibrium swelling degrees and $CO_2$ diffusion coefficients in PBMA and PMMA as measured at a fixed temperature (38°C) and different pressures

| Polymer | Pressure, MPa | $D_1 \times 10^{-10}$, $m^2/s$ | $D' \times 10^{-10}$, $m^2/s$ | Degree of swelling, vol % |
|---|---|---|---|---|
| PBMA | 9 | 5.1 ± 0.2 | 5.8 ± 0.7 | 49 ± 8 |
| | 12.5 | 6.5 ± 0.5 | 4.4 ± 0.4 | 46 ± 7 |
| | 15 | 4.8 ± 1.0 | 4.4 ± 0.4 | 47 ± 10 |
| PMMA | 9 | 1.04 ± 0.10 | 0.51 ± 0.08 | 24 ± 5 |
| | 12.5 | 1.35 ± 0.12 | 0.69 ± 0.09 | 26 ± 8 |
| | 15 | 2.0 ± 0.30 | 0.7 ± 0.30 | 37 ± 5 |

sample in supercritical $CO_2$ makes it possible to measure growth in two linear dimensions; on the basis of these measurements, we drew conclusions on the dynamics of a gain in volume.

An equation of the exact solution to the sorption problem for the time dependence of the sorbate mass in a sample at zero initial and constant boundary conditions is as follows [16, 17]:

$$\frac{M(t)}{M_\infty} = 1 - \frac{512}{\pi^6}\sum_{i=0}^{\infty}\frac{1}{(2i+1)^2}\exp\left(-\frac{\pi^2(2i+1)^2 D't}{l_x^2}\right) \times \sum_{j=0}^{\infty}\frac{1}{(2j+1)^2}\exp\left(-\frac{\pi^2(2j+1)^2 D't}{l_y^2}\right) \times \sum_{k=0}^{\infty}\frac{1}{(2k+1)^2}\exp\left(-\frac{\pi^2(2k+1)^2 D't}{l_z^2}\right), \quad (10)$$

where $M(t)$ is the sorbate mass, $M_\infty$ is the equilibrium mass of the sorbate, and $D'$ is the diffusion coefficient. This equation is valid at $D'$ = const. However, as shown by the numerical experiment (Fig. 2b), Eq. (10) also satisfactorily approximates the calculated functions $M(t)$ with the concentration-dependent diffusion coefficient as defined by Eq. (1) or (2). In this case, the diffusion coefficient $D'$ should be considered an apparent quantity characterizing the rate of sorption by the sample as a whole.

In further analysis using Eq. (1), we assume, like Royer *et al.* [4], that a change in sample volume is proportional to the mass of $CO_2$ sorbed:

$$\frac{V(t) - V_0}{V_\infty - V_0} = \frac{M(t)}{M_\infty}. \quad (11)$$

Here, $V_0$ is the volume of a polymer sample before swelling, $V_\infty$ is the volume of the completely swollen sample, and $M_\infty$ is the equilibrium mass of the sorbate. Then the relative change in sorbate volume is also described by Eq. (10). For example, according to the published data [11], deviation from the linear law for the dependence of the equilibrium mass swelling degree on the volume swelling degree for PMMA at a fixed exposure temperature ($T$ = 35°C) is no more than 7%, which justifies the assumption of Eq. (11).

In essence, the procedure for determining the diffusion coefficient from data on the volume swelling kinetics is analogous to the known approach based on the analysis of the kinetics of movement of a physical (phase) boundary in a polymer during swelling [12, 13]. However, the equations reported in [12, 13] were obtained on the assumption that the mixing of components does not lead to a change in the volume of the system. It is obvious that condition (11) used in this work is less stringent.

The time dependences obtained experimentally for the relative increment in sample volume were approximated by law (10). The task of searching for the best approximation was fulfilled numerically by the least squares procedure, thus allowing the apparent diffusion coefficient of $CO_2$ in a polymer to be found.

Typical swelling curves for PMMA and PBMA are depicted in Fig. 2b; the best approximations of experimental data points by calculated relationship (10) and the values of the diffusion coefficient $D'$ corresponding to these approximations are also shown there. In addition, Fig. 2b presents the results of computational simulation of swelling for two types of concentration dependence of the diffusion coefficient according to laws (1) and (9). It is seen that, in the initial stage (up to approaching diffusion fronts at the sample center, as marked by arrows), Eq. (10) fits the computer simulation results well, also allowing the apparent values of $D'$ to be determined from the approximation. When the apparent values of $D'$ obtained experimentally and by computer simulation are equal, the corresponding dependences of the degree of swelling agree well over the entire time interval (Fig. 2b).

According to the results of computer simulation of type (1) concentration dependence under the conditions $c_x/c_0 = 0.7$ and $D_1/D_2 > 10$, the relationship $D' \simeq 0.5D_1$ holds with good accuracy and the apparent coefficient is $D' \simeq 0.7D_1$ for the concentration dependence of type (9) at $D_1/D_2 > 5$. Both relationships are satisfactorily fulfilled in real experiments with PMMA and PBMA samples, respectively (Tables 1, 2). Thus, these empirical relationships can serve as an additional criterion of adequacy of the models for the concentration dependence of a diffusion coefficient in polymers.

Based on the relationships obtained, we can rewrite law (2) as

$$X^2 = \beta D't \quad (12)$$

and, taking into account the values of $\alpha$ relevant to Eq. (2) ($\simeq$0.7 and $\simeq$0.3 as found for PMMA and PBMA, respectively), can determine the proportionality factor $\beta$ as $\simeq$1.4 and $\simeq$4, respectively. The figures obtained are comparable with the estimate $\beta \simeq 3$ proposed in [12, 13] for determining the apparent diffusion coefficients according to Eq. (12) in systems with limited swelling (Malkin and Chalykh [12] noted that the estimate is true accurate to an order of magnitude). To summarize, we obtained refined values valid for the proposed models of concentration dependence in PMMA (Eq. (1)) and PBMA (Eq. (9)).

### *Analysis of the Dependence of Obtained Diffusion Coefficients and Degrees of Swelling on Exposure Temperature and Pressure*

The results of experiments at different pressures of supercritical $CO_2$ at one temperature (38°C) are presented in Table 1. The figures listed are the mean arithmetic values determined from three to four independent runs. Table 2 presents results obtained at the same pressure (12.5 MPa) and different temperatures. The maximum values of the diffusion coefficient $D_1$ (see Eqs. (1), (9)) were calculated using the procedure of monitoring the movement of optical boundaries: the apparent diffusion coefficient $D'$ (see Eq. (10)) was determined from the analysis of the swelling kinetics (movement of phase boundaries).

The results obtained show that the diffusion coefficients ($D_1$, $D'$) and equilibrium degrees of swelling for the samples examined depend on the conditions of their exposure to supercritical $CO_2$.

For PMMA, it was found that the diffusion coefficients increased by a factor of 1.5–2 with increasing pressure from 9 to 15 MPa; as the temperature in the cell increased from 38 to 65°C, the diffusion coefficient in PMMA increased by 20–40%.

The results obtained for PBMA do not permit us to draw an unambiguous conclusion as to the character of the pressure dependence for the diffusion coefficient. At the same time, it turned out that the diffusion coefficient in PBMA also increased by 50–80% with increasing temperature in the cell from 38 to 65°C.

A somewhat larger statistical scatter of the results for PBMA can be explained as follows. The diffusion coefficient in PBMA is approximately an order of magnitude greater than that in PMMA; therefore, the diffusion processes occur at a substantially higher rate. According to Eq. (10), the characteristic time of diffusion is defined by $\tau = l_{\text{eff}}^2/\pi^2$, where the effective size $l_{\text{eff}}$ is related to the linear dimensions of a sample by $\frac{1}{l_{\text{eff}}^2} = \frac{1}{l_x^2} + \frac{1}{l_y^2} + \frac{1}{l_z^2}$. The use of these relationships yields characteristic diffusion times of 5–10 min and ~1 h for the PBMA and PMMA samples, respectively. Consequently, the major portion of $CO_2$ enters PBMA samples within the first minutes of an experimental run. In affecting sorption processes, density and temperature fluctuations in the initial stage of exposure, which are due to the perturbation of the supercritical fluid during its admittance to the cell, can introduce a greater error into measured values only in the case when the characteristic diffusion times are shorter than or comparable to the relaxation times of initial perturbations (as observed for PBMA samples).

**Table 2.** Equilibrium swelling degrees and $CO_2$ diffusion coefficients in PBMA and PMMA as measured at a fixed pressure (12.5 MPa) and different temperatures

| Polymer | Temperature, °C | $D_1 \times 10^{-10}$, $m^2/s$ | $D' \times 10^{-10}$, $m^2/s$ | Degree of swelling, vol % |
|---|---|---|---|---|
| PBMA | 50 | 6.6 ± 0.7 | 7.2 ± 1.0 | 21 ± 6 |
| | 55 | 10 ± 3 | 6.4 ± 1.3 | 34 ± 3 |
| | 65 | 10 ± 2 | 8 ± 2 | 31 ± 6 |
| PMMA | 50 | 1.4 ± 0.2 | 0.69 ± 0.10 | 32 ± 6 |
| | 65 | 1.6 ± 0.3 | 0.99 ± 0.12 | 10 ± 4 |

The analysis of the values measured for the equilibrium volume swelling degree (Table 1 and 2) shows that the degree of swelling of PMMA at a fixed exposure temperature (38°C) increases with increasing pressure. At a fixed pressure (12.5 MPa) and temperature elevation from 38 to 65°C, the degree of swelling of PMMA passes through a maximum (50°C) and then decreases. These results are consistent with the data obtained by Wissinger and Paulaitis [9], who studied PMMA swelling in $CO_2$ at pressures of up to 10 MPa. They also noticed an increase in the degree of swelling with increasing pressure and its nonmonotonic dependence on temperature: as the temperature increased from 33 to 42°C (at a pressure of 10 MPa), the degree of swelling increased from ~20 to ~29%, the further increase in temperature decreased the swelling from ~29 to ~26%. Similar nonmonotony of the dependence of swelling on temperature in glassy polymers has also been described by von Schnitzler and Eggers [5].

### *Porous Structure Formation*

As one can see from the data presented in Fig. 1, there is no porous structure that could have been formed in the samples during $CO_2$ sorption. Pores in PMMA and PBMA are produced only in the $CO_2$ desorption process after preliminary exposure under

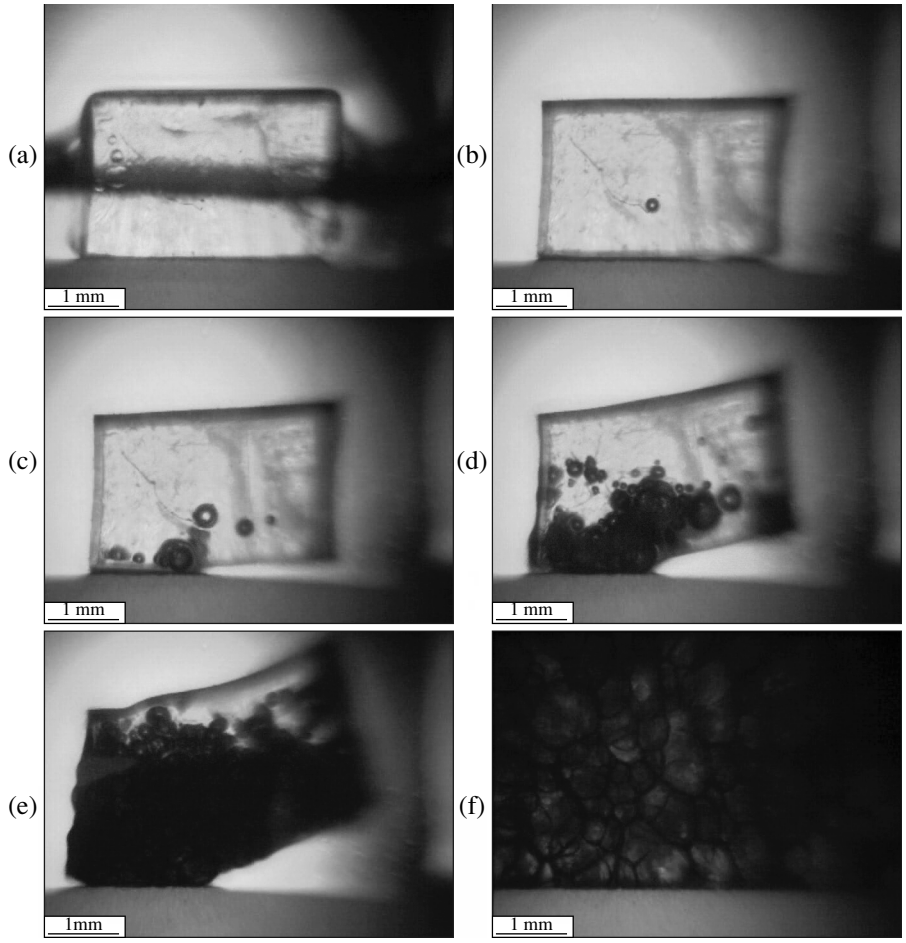


**Fig. 4.** Changes inn PBMA morphology during $CO_2$ desorption. The sample was preliminarily exposed to supercritical $CO_2$ at 38°C and 9 MPa. Before the desorption, the cell was cooled to 25°C (the meniscus of liquid $CO_2$ is detectable in Fig. 4a). Desorption time: (a) 0, (b) 25, (c) 30, (d) 34, (e) 37, and (f) 60 s.

supercritical conditions. Figure 4 give the images of the pore formation steps in PBMA.

It has been found that, if the cell temperature is lowered to room temperature (~20°C) prior to desorption and a constant pressure is maintained, no porous structure is formed in PMMA. We assume that this is due to the transition of PMMA to the glassy state upon the decrease in temperature to room temperature, which impedes pore formation. At the same time, under decompression conditions after lowering the temperature for PBMA samples, the pore formation proceeds even more intensely as compared to that upon decompression without a preliminary decrease in temperature. Along with the increase in the degree of swelling with lowering the temperature, this effect seems to be due to the fact that, unlike PMMA, swollen PBMA remains in the rubbery state at room temperature as well.

In order to reveal the influence of exposure conditions on the pore formation character and the morphology of pores produced in the polymers of interest, we examined the outer and cleaved surfaces of samples by the AFM technique.

In the examination of PBMA, it was found that, after completion of the sorption–desorption cycle for supercritical $CO_2$, a significant amount of clearly marked pores with pit geometry is formed on the sample surface, the depth and diameter of the pores varying from tens and hundreds of nanometers to a few micrometers (pores with a depth of greater than 2–3 μm could not be adequately visualized with the microscopic probe because of the limited dynamic range of the scanner). The AFM technique made it possible to exhibit differences in the surface morphology of PBMA samples exposed under different conditions. The number and characteristic size of pores detected on the polymer surface turned out to depend on the temperature and pressure maintained during the exposure of the polymer to supercritical $CO_2$. Figure 5 presents the results of the AFM study of PBMA samples exposed at the same temperature (38°C) and various pressures (15–25 MPa). It is seen that the greatest amount of pores is formed at a

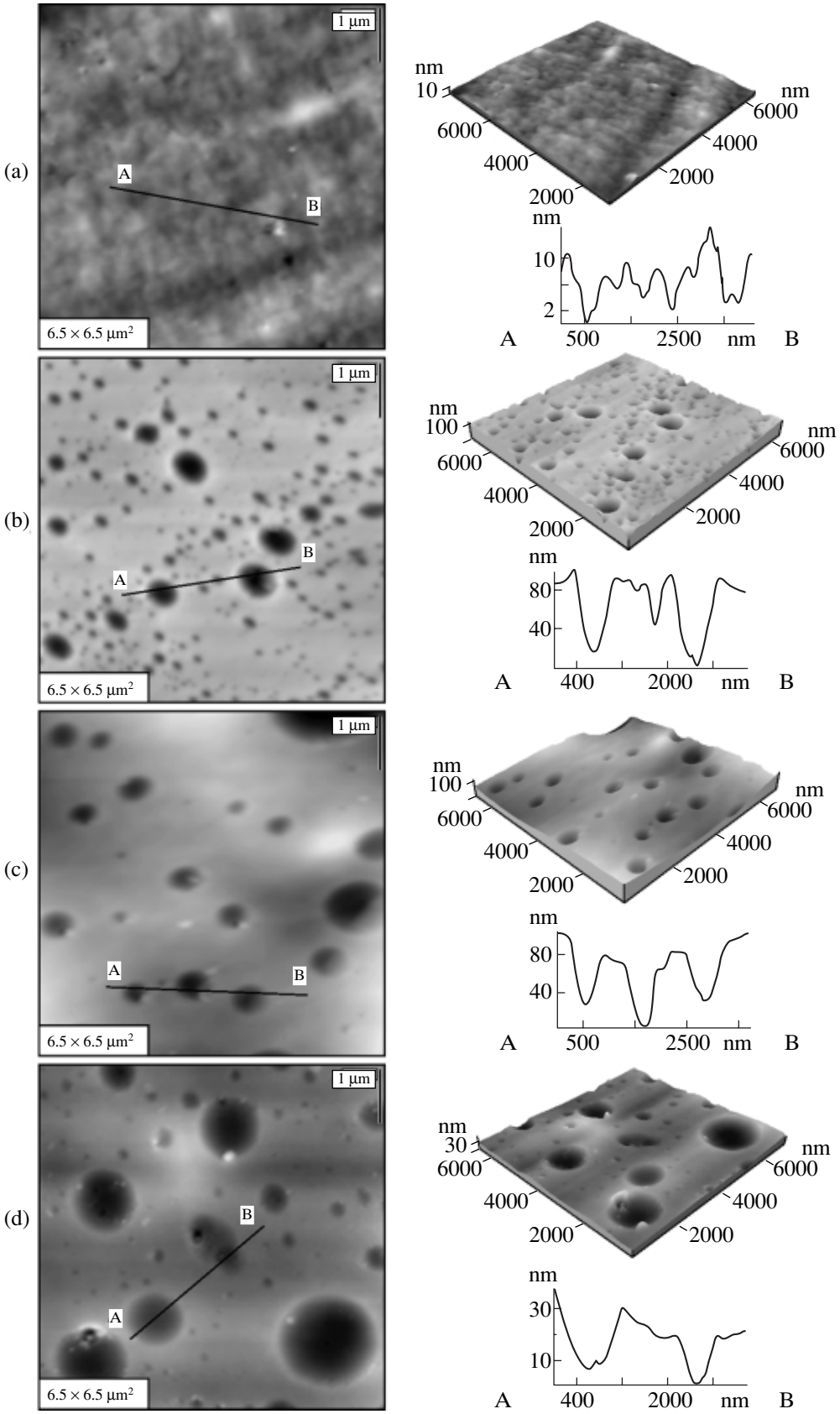


**Fig. 5.** AFM images of the PBMA surface (a) in the virgin state and after exposure to supercritical $CO_2$ at (b) 38°C and 15 MPa, (c) 38°C and 25 MPa, and (d) 70°C and 8 MPa.

pressure of 15 MPa (Fig. 5b), the pores having a very broad size distribution (diameter 0.2–2 μm, depth 1–100 nm). After exposure at higher (25 MPa, as shown in Fig 5c) or lower (8 MPa—no image is given) pressures, the number of pores formed is smaller. However, if the temperature in the cell is elevated to 50–70°C at a pressure of 8 MPa (Fig. 5d), the surface of the exposed polymer will also contain a considerable amount of pores with a broad size distribution.

At the same time, a certain region near the surface of PMMA samples usually remains free of pores (unlike the case of PBMA). We explain this behavior (the absence of pores on the surface and near it) by the fact that, during decompression, PMMA undergoes glass transition near the surface; therefore, the pore formation process takes place only in deeper regions of the sample.

## CONCLUSIONS

In this work, we studied the swelling of PBMA and PMMA samples in situ. Based on the analysis of the movement of optical boundaries and the kinetics of swelling, the diffusion coefficients of $CO_2$ in the polymers were calculated. The equilibrium degrees of swelling were determined. The specific features of formation of optical boundaries observed in the experiments with PMMA and PBMA were explained in a comparative analysis, which comprised fitting to computer simulation results, thus allowing us to conclude on the character of the concentration dependence of the diffusion coefficients of $CO_2$ in these polymers.

According to the model proposed for PMMA, the diffusion coefficient increases dramatically, by more than an order of magnitude, when the sorbate concentration reaches a certain limit (~70% of the equilibrium value). We assume that the polymer undergoes a transition from the glassy to the rubbery state at this concentration of $CO_2$ sorbed under the given experimental conditions. In the model for PBMA, the diffusion coefficient is supposed to increase gradually (5–10 times in total), thus resulting in the development of an optical boundary of another form than in the case of PMMA.

The effects of temperature and pressure on the obtained values of the degrees of swelling and $CO_2$ diffusion coefficients in the polymers were analyzed; the results obtained agree with the published data, thus indicating the adequacy of the optical procedure used for the first time to study polymer swelling in a supercritical fluid.

Using the techniques of optical and atomic-force microscopy, the morphology of porous structures produced in the samples upon $CO_2$ desorption was characterized. The nonoccurrence of pore formation processes in PMMA in near-surface regions or throughout the bulk (upon $CO_2$ desorption at a reduced temperature) is explained by the glass transition of the polymer.

## REFERENCES

1. Cooper, A.I., *J. Mater. Chem.*, 2000, vol. 10, p. 207.
2. Kendall, J.L., Canelas, D.A., Young, J.L., and DeSimone, J.M., *Chem. Rev.*, 1999, vol. 99, no. 2, p. 543.
3. McHugh, M.A. and Krukonis, V.J., *Supercritical Fluid Extraction*, Stoneham: Butterworth-Heinemann, 1994.
4. Royer, J.R., DeSimone, J.M., and Khan, S.A., *Macromolecules*, 1999, vol. 32, no. 26, p. 8965.
5. Schnitzler von, J. and Eggers, R., *J. Supercrit. Fluids*, 1999, vol. 16, p. 81.
6. Popov, V.K., Bagratashvili, V.N., Krasnov, A.P., Said-Galiyev, E.E., Nikitin, L.N., Afonicheva, O.V., and Aliev, A.D., *Tribology Lett.*, 1998, no. 5, p. 297.
7. Sobol', E.N., Bagratashvili, V.N., Popov, V.K., Sobol', A.E., Said-Galiev, E.E., and Nikitin, L.N., *Zh. Fiz. Khim.*, 1998, vol. 72, no. 1, p. 23.
8. Filonov, A.S., Gavrilko, D.Yu., and Yaminsky, I.V., *Programmnoe obespechenie "FemtoSkan" dlya obrabotki trekhmernykh izobrazhenii* (FemtoScan SPM Image Processing Manual), Moscow: Advanced Technologics Center, 2001.
9. Wissinger, R.G. and Paulaitis, M.E., *J. Polym. Sci., Part B: Polym. Phys.*, 1987, vol. 25, p. 2497.
10. Kikic, I., Lora, M., Cortesi, A., and Sist, P., *Fluid Phase Equilibr.*, 1999, vols. 158–160, p. 913.
11. Zhang, Y., Gangwani, K.K., and Lemert, R.M., *J. Supercrit. Fluids*, 1997, vol. 11, p. 115.
12. Malkin, A.Ya. and Chalykh, A.E., *Diffuziya i vyazkost' polimerov: metody izmereniya* (Diffusion and Viscosity of Polymers: Measurement Techniques), Moscow: Khimiya, 1979.
13. Vasenin, R.M., Chalykh, A.E., and Korobko, V.I., *Vysokomol. Soedin.*, 1965, vol. 7, no. 4, p. 593.
14. Chiou, J.S., Barlow, J.W., and Paul, D.R., *J. Appl. Polym. Sci.*, 1985, vol. 30, p. 2633.
15. Wang, W.-Ch.V., Kramer, E.J., and Sachse, W.H., *J. Polym. Sci., Part B: Polym. Phys.*, 1982, vol. 20, p. 1371.
16. Carslaw, H.S. and Jaeger, J.C., *Conduction of Heat in Solids*, Oxford: Clarendon, 1959.
17. Crank, J., *The Mathematics of Diffusion*, Oxford: Clarendon, 1975.
18. Born, M. and Wolf, E., *Principles of Optics*, London: Pergamon, 1968.
19. Press, W.H., Teukolsky, S.A., Vetterling, W.T., and Flannery, B.P., *Numerical Recipes in C. The Art of Scientific Computing*, Cambridge: Cambridge Univ. Press, 1992.
20. Askadskii, A.A. and Kondrashenko, V.I., *Computer-Based Materiology of Polymers*, Moscow: Scientific World, 1999, vol. 1.
21. Marioth, E., Koenig, B., Krause, H., and Loebbecke, S., *Ind. Eng. Chem. Res.*, 2000, vol. 39, p. 4853.